

Two-Stage Framework for Efficient UAV-Based Wildfire Video Analysis with Adaptive Compression and Fire Source Detection

Yanbing Bai^{*}, *Member, IEEE*, Rui-Yang Ju^{*}, *Student Member, IEEE*, Lemeng Zhao^{*}, Junjie Hu, Jianchao Bi, Erick Mas, Shunichi Koshimura[†]

Abstract—Unmanned Aerial Vehicles (UAVs) have become increasingly important in disaster emergency response by enabling real-time aerial video analysis. Due to the limited computational resources available on UAVs, large models cannot be run independently for real-time analysis. To overcome this challenge, we propose a lightweight and efficient two-stage framework for real-time wildfire monitoring and fire source detection on UAV platforms. Specifically, in Stage 1, we utilize a policy network to identify and discard redundant video clips using frame compression techniques, thereby reducing computational costs. In addition, we introduce a station point mechanism that leverages future frame information within the sequential policy network to improve prediction accuracy. In Stage 2, once the frame is classified as “fire”, we employ the improved YOLOv8 model to localize the fire source. We evaluate the Stage 1 method using the FLAME and HMDB51 datasets, and the Stage 2 method using the Fire & Smoke dataset. Experimental results show that our method significantly reduces computational costs while maintaining classification accuracy in Stage 1, and achieves higher detection accuracy with similar inference time in Stage 2 compared to baseline methods.

Index Terms—Frame selection, video compression, UAV-based video analysis, wildfire monitor, wildfire detection

I. INTRODUCTION

Forest fires pose a serious threat to both human life and the ecological environment, and have attracted growing attention in recent years [1]. In particular, UAV-based platforms have become increasingly popular in disaster monitoring and response due to their ability to capture real-time and efficient ground information efficiently [2]–[5]. UAV-based platforms not only accelerate data acquisition but also reduce the risks involved in manual inspection, thereby enhancing safety in forest fire management.

In recent years, several studies have utilized visual cues such as flames [6] and smoke [7]–[9] for wildfire detection. While these methods are feasible, performing fire source detection across an entire video is computationally inefficient,

especially considering the associated processing costs and the low probability of wildfire occurrence. A more efficient strategy is to first detect the presence of fire in UAV-based video streams, and only localize the fire source once fire is confirmed.

Therefore, based on our adaptive clip-aware compression and frame selection method for UAV-collected wildfire videos proposed in the conference paper [10], we extend the method into a practical application by introducing a lightweight and efficient two-stage framework. In Stage 1, we perform frame selection on UAV-based video streams to identify frames containing potential wildfire activity. In Stage 2, for frames classified as containing fire, we apply an improved YOLOv8 (You Only Look Once, Version 8) model to accurately localize the fire source.

The proposed method in Stage 1 focuses on video understanding, a topic of increasing interest in the field of video streaming data analysis [1]. Real-time processing of video streams in disaster response scenarios presents significant computational challenges [11]. To address this, researchers have explored methods to reduce computational costs, such as the development of lightweight architectures [12]–[14] and the selection of representative frames [15]–[17]. Inspired by these advancements, we propose a novel method in Stage 1: the adaptive clip-aware compression and frame selection network. Unlike traditional methods [6], [18], which analyze videos on a frame-by-frame basis, our method combines multiple clips into a single frame. The decision of when to merge clips is guided by video features, enabling more informed choices. By allocating computational resources to information-rich frames and discarding less relevant clips, our method effectively reduces computational costs while maintaining classification accuracy.

Aerial videos [19], [20] are often captured under challenging conditions, including blurred frames and abrupt changes caused by unpredictable camera vibrations from air currents. To address these issues, we propose a station point mechanism that incorporates features from future frames, allowing the policy network to make more informed and stable decisions during aerial video processing. In addition, we introduce a frame selection module, where the policy network determines the importance of each frame. This module assigns scores to individual frames and selects the highest-scoring ones to reconstruct a concise video. The process requires no complex pre-processing or post-processing, resembling the editing of a long video to create a shorter, more informative summary. The resulting video preserves critical temporal and spatial information, essential for effective disaster monitoring.

This paper is an extended version of a paper presented at the 2024 IEEE/RSJ International Conference on Intelligent Robots and Systems (IROS), held on October 14–18, 2024, in Abu Dhabi, United Arab Emirates.

Yanbing Bai and Lemeng Zhao are with the Center for Applied Statistics, School of Statistics, Renmin University of China, Beijing 100872, China.

Rui-Yang Ju is with the Graduate Institute of Networking and Multimedia, National Taiwan University, Taipei 106335, Taiwan.

Junjie Hu is with the Shenzhen Institute of Artificial Intelligence and Robotics for Society, Shenzhen 518129, China.

Jianchao Bi is with the Gaoling School of Artificial Intelligence, Renmin University of China, Beijing 100872, China.

Erick Mas and Shunichi Koshimura are with the International Research Institute of Disaster Science, Tohoku University, Sendai 980-8572, Japan.

^{*}These authors contributed equally to this work.

[†]Corresponding author: Shunichi Koshimura (koshimura@tohoku.ac.jp).

For frames classified as containing fire, we process them further in Stage 2. YOLOv8 [21], a widely used lightweight object detection model, is well-suited for UAV platforms. We improve the architecture of YOLOv8 models by integrating attention mechanisms to enhance the accuracy of fire source localization.

The main contributions of this work are as follows:

- We propose a lightweight and efficient two-stage framework for wildfire monitoring and fire source detection. This framework processes aerial video of wildfire scenes, performing both frame selection and wildfire classification. In addition, for frames classified as containing fire, the framework further localizes the fire source.
- In Stage 1, which focuses on UAV-based wildfire video understanding and frame selection, we introduce a station point mechanism that provides additional spatio-temporal features, enhancing the model's efficiency, robustness, and classification accuracy compared to the baseline method.
- In Stage 2, for fire source detection, we integrate attention mechanisms into the YOLOv8 model to achieve higher detection accuracy compared to the baseline model.

II. RELATED WORK

A. Video Understanding

Efficient video understanding models based on representative frames provide feasible solutions to the high computational costs associated with video analysis [22]. Two primary techniques are used for video frame selection: serial (sequential) sampling and parallel sampling.

In serial sampling, frames are processed in temporal order, with a learned policy determining which frame to process next. AdaFrame [23] utilized a memory-augmented Long Short-Term Memory (LSTM) network to retain both temporal and spatial information, using hidden states to guide frame selection. VideoIQ [24] reduced computational overhead by dynamically allocating variable bits or adjusting input resolution on a per-frame basis.

In contrast, parallel sampling processes frames or video clips independently and aggregates the results. SCSampler [25] scored fixed-length clips and synthesized predictions accordingly. OCSampler [22] applied a simple one-step reinforcement learning strategy to directly select a comprehensive set of features for video-level modeling.

In addition, recent methods have introduced novel methods to temporal representation. For instance, AdaFuse [26] dynamically fused channels from current and past feature maps to improve temporal modeling. However, these methods primarily focused on general video understanding tasks and were typically evaluated on standard benchmark datasets such as ActivityNet [27], FCVID [28], and Kinetics [29]. As a result, these methods have not been evaluated for UAV-based wildfire videos, which present unique challenges such as sparse informative frames, dynamic smoke patterns, and complex backgrounds.

B. Frame Selection

Frame selection is crucial for efficient video understanding. Methods such as AdaFrame [23], Frame Glimpse [30], and SCSampler [25] employed frame sampling strategies combined with policy networks to identify the most informative frames or clips within a video sequence. These selected frames were then used to construct clips for various recognition tasks. SMART [31] utilized a hierarchical selection method, first computing spatial classification scores with a single-frame selector, followed by a global selector that captured both temporal and spatial category information from frame pairs. The final selection was determined by combining these two scores for each frame.

In contrast, MGSampler [32] focused on motion salience by utilizing two types of motion representations (motion-sensitive and motion-uniform) to effectively distinguish salient motion frames from the background. It employed a motion-uniform sampling strategy based on cumulative motion distribution to ensure that the selected frames comprehensively covered all critical clips with high motion dynamics.

C. Object Detection

For object detection tasks, You Only Look Once (YOLO) is one of the most popular lightweight models due to its balance between model size and accuracy. With the introduction of YOLOv8 [21], it has been widely adopted in various object detection applications, including fire detection. Casas *et al.* [33] evaluated the performance of YOLOv5, YOLOv6, YOLOv7, YOLOv8, and YOLO-NAS in detecting smoke and wildfires using the Foggia dataset. Similarly, Ramos *et al.* [34] evaluated YOLOv8, YOLOv9, YOLOv10, and YOLOv11 on the Fire and Smoke dataset for wildfire and smoke detection. These works did not propose improvements to the YOLO model architecture, despite evaluating several models from the YOLO series.

D. Attention Mechanism

The attention mechanism is an effective method to improve the performance of YOLO series models. Hu *et al.* [35] introduced Squeeze-and-Excitation Networks (SE-Nets), which significantly improved model performance by generating channel weights through global average pooling, fully connected layers, and Sigmoid functions. Woo *et al.* [36] combined channel and spatial attention to propose the Convolutional Block Attention Module (CBAM), further enhancing the representation capability of Convolutional Neural Networks (CNNs). Wang *et al.* [37] proposed Efficient Channel Attention (ECA), which improved performance with fewer parameters by focusing on channel relationships. In contrast, Zhang *et al.* [38] introduced Shuffle Attention (SA), which grouped channel features and integrated complementary features using a Shuffle Unit, achieving excellent results with low model complexity. These attention modules can be applied to various neural network architectures to enhance performance.

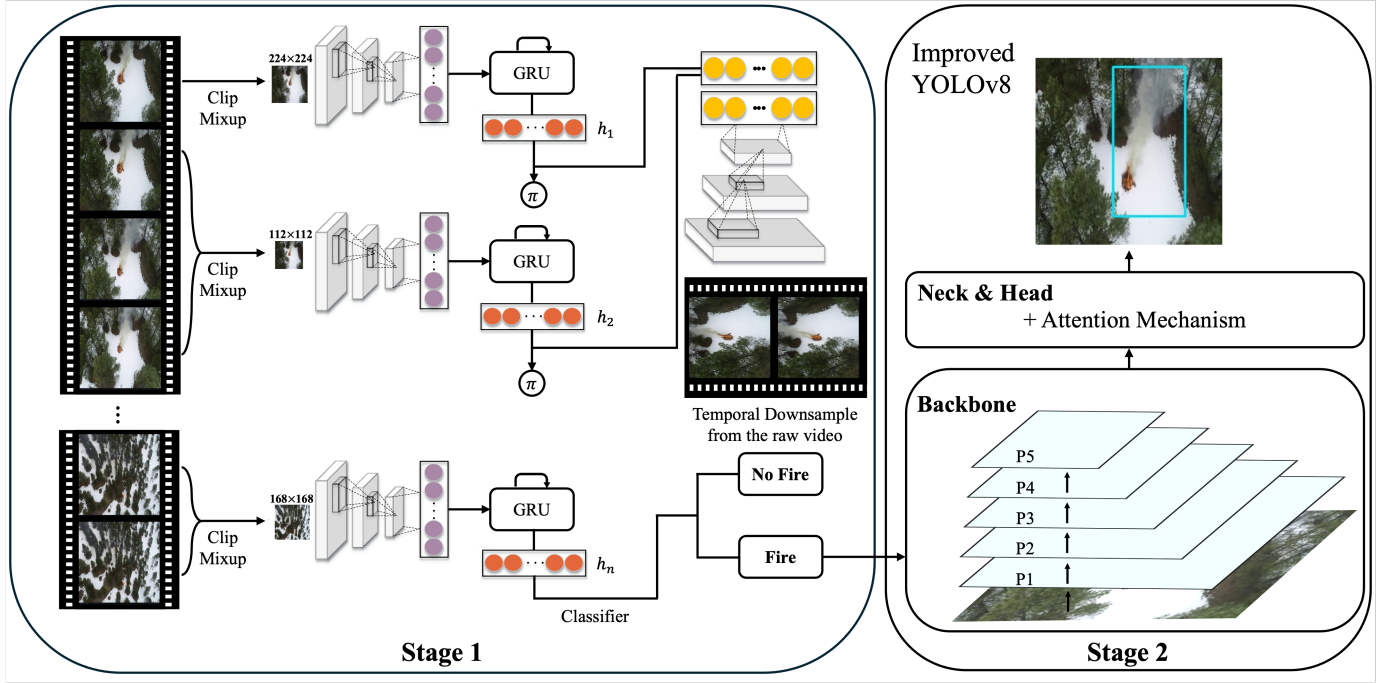


Fig. 1. Pipeline of the proposed two-stage framework. In Stage 1, frame selection is performed based on a static distribution guided by π . Our method enables efficient video understanding by compressing uninformative clips and utilizing extracted features to select informative frames for dataset distillation. In Stage 2, the improved YOLOv8 models are employed to accurately localize the fire source.

III. METHOD

A. Two-Stage Framework

The pipeline of the proposed two-stage framework is shown in Fig. 1. In Stage 1, given a video v composed of a sequence of frames $X = x_{t=1}^N$, where N denotes the total number of frames and t represents the current time step, the processing begins at $t = 1$. At this initial step, our method uniformly samples multiple station points from the input and extracts their features using a 2D-CNN, denoted as s_m . These station point features provide future context for the policy network π .

At each subsequent time step $t = i$, the policy network π receives as input the concatenation of clip-level features from the feature extraction network f_s and the corresponding station point features. Based on this input, π evaluates the importance of upcoming frames and determines the number of frames to compress at $t = i + 1$.

After the entire video has been processed, the classifier f_c performs video classification. Frame selection is performed statically and guided by the pre-trained policy network π , which effectively estimates the importance of future frames. Each frame is assigned a score according to the output of π .

In Stage 2, object detection is performed on these frames classified as containing wildfire. We employ an improved YOLOv8 model, integrated with attention mechanisms, to accurately localize the fire source within these frames.

B. Stage 1

1) *Clip Mixup*: Mixup [39] is a data augmentation technique that generates new training samples by linearly inter-

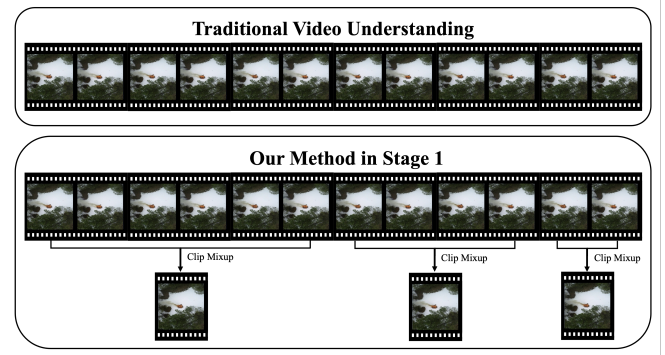


Fig. 2. Comparison between the traditional method and our method for video understanding. Traditional method analyzes videos frame by frame, and our method employs a clip mixup strategy that merges multiple clips by leveraging video features.

polating between two inputs and their corresponding labels within the same batch. The equations are as follows:

$$x' = \lambda x_i + (1 - \lambda)x_j, \quad (1)$$

$$y' = \lambda y_i + (1 - \lambda)y_j, \quad (2)$$

where x_i and x_j are input samples, and y_i and y_j are their corresponding labels. The mixing coefficient λ is drawn from a Beta distribution, $Beta(\alpha, \alpha)$.

In our framework, we adopt a variant of this method, referred to as clip mixup, to improve computational efficiency while preserving essential video content, as shown in Fig. 2. As video classification does not require frame-level annotations, we apply only Eq. (1). Specifically, for input clips containing multiple frames, clip mixup fuses the first and last

frames to generate a single representative frame, denoted as x_i^{mixup} . This design is motivated by the observation that frames within a short clip tend to be visually similar, allowing the merged frame to serve as an effective proxy for the entire clip.

2) *Feature Extraction Network*: At each time step $t = i$, the input frame x_i^{mixup} is first processed by the CNN to extract spatial features, which are then fed into the RNN. The hidden state of the RNN at time step i , denoted as h_i , captures the accumulated video information up to that point. Formally, this process is defined as:

$$h_i = f_s(x_i^{\text{mixup}}), \quad (3)$$

where h_i serves as a compact representation of the video content observed up to time i , and is subsequently utilized by the policy network π for decision making.

3) *Policy Network*: The policy network π determines the number of frames to be fused at the next time step by selecting an action k_i from a discrete action space A . Upon receiving the hidden state h_i from the feature extractor f_s at time $t = i$, π identifies the nearest future station point feature s_m^{nearest} from the set s_m . The hidden state and the selected station point feature are concatenated and fed into π , which outputs a predicted probability distribution a_i^p over the action space A :

$$a_i^p = \text{softmax}(\pi([h_i : s_m^{\text{nearest}}])). \quad (4)$$

The action space is defined as $A = 1, 3, 5, 7$. Selecting an action $k_i \in A$ at time $t = i$ means that k_i frames will be merged into a single frame via clip mixup at time $t = i + 1$. A smaller value of k_i indicates that the current clip is more informative and thus requires higher temporal resolution.

To further optimize resource allocation, frames of varying importance levels are resized to different resolutions. We define the resolution set as $R = 224, 168, 112, 84$, where each resolution corresponds to a specific action in A . This mapping allows π to dynamically adjust the level of feature detail based on predicted importance. For instance, if the policy determines that current features are sufficient, it may merge five or seven frames at a lower resolution; conversely, when finer details are needed, it several frames at a higher resolution.

The architecture of π consists of a Group Normalization [40] layer followed by a fully connected layer. The use of Group Normalization accelerates convergence during training by stabilizing feature distributions.

4) *Frame Selection*: The policy network π effectively evaluates the importance of video frames, as reflected by its fusion decisions: the greater the number of frames fused, the less important they are considered. To quantify this, we introduce a preference score S to evaluate the significance of each frame.

According to Eq. (4), at time step $t = i$, the policy network outputs a probability distribution over the action space A , denoted as $p_i = a_{ij}^p$, where $1 \leq j \leq \|A\|$. For the clip to be fused at $t = i + 1$, denoted as clip_{i+1} , we define its preference score S_{i+1} as:

$$S_{i+1} = \sum_{j=1}^{\|A\|} \frac{a_{ij}^c}{A_j}, \quad (5)$$

where $c \in \{p, gm, gs\}$ denotes different variants of the score.

To further refine the preference score S at the frame level, the central frame of the clip is assigned the full score S_i , with a gradual decay of 10% applied symmetrically toward the neighboring frames.

5) *Gumbel Softmax Trick*: The action space A is discrete, which poses challenges for optimization via gradient backpropagation. In such cases, reinforcement learning is commonly employed to train the policy network. However, reinforcement learning often suffers from slow convergence across a wide range of applications [41]. To address this limitation, we adopt the Gumbel Softmax trick [42], which enables direct optimization of the policy network through gradient-based methods.

The Gumbel Softmax is an effective reparameterization technique that transforms previously non-differentiable categorical distributions into differentiable approximations, introducing stochasticity during training and encouraging exploration. Specifically, the policy network selects actions using the Gumbel Max operation rather than the non-differentiable $\arg \max$ [42]:

$$a_i^{gm} = \arg \max (\log(a_i^p) + G_i), \quad (6)$$

where $G_i = -\log(-\log(U_i))$, and $U_i \sim \text{Uniform}(0, 1)$.

For backpropagation, a differentiable Gumbel-Softmax approximation is used to approximate the $\arg \max$ operation and enable gradient computation:

$$a_i^{gs} = \text{softmax} \left(\frac{\log(a_i^p) + G_i}{\tau} \right), \quad (7)$$

where τ is the softmax temperature hyperparameter. When $\tau > 0$, the output is a smooth distribution; as $\tau \rightarrow 0$, it converges to one-hot vectors. Following prior works [16], [24], we initialize τ at 5 and gradually anneal it to 0 over the course of training.

C. Stage 2

1) *Baseline Model*: The architecture of the baseline model (i.e., YOLOv8) consists of Backbone, Neck, and Head, as illustrated in Fig. 1. The Backbone adopts the Cross Stage Partial (CSP) structure [43], which reduces computational cost while improving the learning capability of the CNNs. Compared to YOLOv5 [44], YOLOv8 introduces a new Coarse-to-Fine (C2f) module, replacing the previously used Concentrated-Comprehensive Convolution (C3) module. C2f integrates the C3 design with the Extended ELAN (E-ELAN) concept [45] from YOLOv7 [46], and comprises two convolutional blocks connected by multiple bottlenecks, each implemented as a Convolution–BatchNorm–SiLU (CBS).

For the Neck architecture, YOLOv8 retains the Feature Pyramid Network (FPN) [47] and Path Aggregation Network (PAN) [48] structure adopted from YOLOv5. The FPN enhances low-level features via up-sampling, while the PAN strengthens high-level localization through down-sampling. This combination improves the model's ability to detect objects across multiple scales. In addition, YOLOv8 removes redundant convolutional operations during the up-sampling stage to further improve inference efficiency.

In the Head design, YOLOv8 adopts a decoupled architecture, separating classification and regression branches to improve task-specific learning performance. Moreover, the Objectness branch is removed, leaving only classification and regression outputs. YOLOv8 also transitions from an anchor-based method [49] to an anchor-free model [50], which directly predicts the object centroid and its boundary offsets for localization.

2) *Attention Module*: Ju *et al.* [51], [52] propose YOLOv8-AM and apply it to pediatric wrist fracture detection, achieving impressive results. In this work, we adopt these improved YOLOv8 models to wildfire images captured by UAVs and further extend them to enable localize the fire sources. Specifically, we employ three variants: YOLOv8+ResCBAM (Res-Block + CBAM), YOLOv8+ECA, and YOLOv8+SA.

As illustrated in Fig. 1, we integrate the attention modules into the Neck of YOLOv8. In particular, one attention module is added after each of the four C2f modules, with the specific module selected from ResCBAM, ECA, or SA, depending on the variant.

Convolutional Block Attention Module (CBAM) [36] is a lightweight and effective attention mechanism composed of two sequential sub-modules: channel attention and spatial attention. It enhances feature representation by adaptively refining both the channel-wise and spatial-wise focus of the network. CBAM is well-suited for wildfire detection, where precise localization of small and irregular fire regions is essential. By sequentially applying channel and spatial attention, CBAM enables YOLOv8 to better capture fire-related features, such as subtle color or texture variations, while suppressing irrelevant background noise often present in the aerial images. Integrating CBAM into the Neck of YOLOv8 allows the model to adaptively enhance the most discriminative intermediate features before detection, improving the accuracy of fire source localization.

Efficient Channel Attention (ECA) module [37] is a lightweight attention mechanism designed to capture essential inter-channel dependencies while minimizing computational and parameter overhead. Unlike traditional attention mechanisms that rely on dimensionality reduction, which may lead to information loss, ECA employs a 1D convolutional operation to model local cross-channel interactions after global average pooling. For wildfire source localization using based on the UAV images, accurate detection of fire regions requires heightened sensitivity to subtle variations in color, brightness, and texture, features often encoded in the channel dimension. By integrating ECA into the Neck of YOLOv8, the model can more effectively highlight channel-wise features that are relevant to fire patterns, while suppressing less informative responses.

Shuffle Attention (SA) module [38] is an efficient attention mechanism that integrates both channel and spatial attention through feature grouping and channel shuffling. This module fuses the enhanced channel and spatial features and redistributes them through channel shuffling, enabling effective cross-group information exchange and holistic feature refinement. Wildfire scenes often exhibit complex spatial patterns, such as scattered flames, diffuse smoke, and varying vegetation

Algorithm 1 Training procedure of our method in Stage 1

Require: A set of videos V , action space A , feature extractor f_s , policy π , classifier f_c , Gumbel Max $\text{GM}(\cdot)$, Clip Mixup $\text{cm}(\cdot)$

- 1: **for** each video $v \in V$ **do**
- 2: Sample station point features s_m from v
- 3: $L \leftarrow \text{len}(v)$, $l \leftarrow 0$
- 4: Initialize $x^{\text{mixup}} \leftarrow v[0]$
- 5: **while** $l < L$ **do**
- 6: $h \leftarrow f_s(x^{\text{mixup}})$
- 7: Find s_m^{nearest} such that $m > l$ and $|m - l|$ is minimal
- 8: $a^{\text{gm}} \leftarrow \text{GM}(\pi([h : s_m^{\text{nearest}}]))$
- 9: $N \leftarrow \min(L - l, A[a^{\text{gm}}])$
- 10: $x^{\text{mixup}} \leftarrow \text{cm}(v[l : l + N])$
- 11: $l \leftarrow l + N$
- 12: $h_{\text{final}} \leftarrow h$
- 13: **end while**
- 14: $p \leftarrow f_c(h_{\text{final}})$
- 15: Compute losses L_c, L_b, L_g (Eqs. (9)–(11))
- 16: $L \leftarrow \text{total loss}$ (Eq. (8))
- 17: Update f_s, π, f_c by minimizing L
- 18: **end for**

textures, which necessitate the joint modeling of channel-wise semantics and spatial locality. By applying SA in the Neck of YOLOv8, the model gains the ability to capture fine-grained regional cues and their broader contextual relationships.

D. Training Procedure

The complete training process of our method in Stage 1 is detailed in Algorithm 1. The algorithm describes an iterative procedure that begins with sampling video data, followed by feature extraction using a combined CNN–RNN backbone. The policy network π is then used to dynamically determine the optimal number of frames to compress through clip mixup. To enable robust and differentiable action selection, the process incorporates Gumbel-Max sampling. This is followed by clip compression, which improves computational efficiency while preserving essential video information.

Finally, the classifier network f_c predicts the video label. The entire model, including the feature extractor, policy network, and classifier, is jointly optimized by minimizing a composite loss function. This systematic method enables efficient and adaptive video understanding, making it well-suited for wildfire monitoring applications.

E. Loss Function

1) *Stage 1*: We design three loss components to train the model in Stage 1, and define the total loss L as follows:

$$L = L_c + \beta L_b + \gamma L_g, \quad (8)$$

where β and γ are hyperparameter that balance the contributions of each loss term. In our experiments, we set $\beta = 0.3$ and $\gamma = 0.1$, following the settings used in VideoIQ [24].

The first component, cross-entropy loss L_c , measures the classification error between the predicted output and the ground truth:

$$L_c = \mathbb{E} \left[-Y \log(f_c(h_{\text{final}})) \right], \quad (9)$$

where h_{final} denotes the final hidden state produced by the feature extraction network.

To prevent the policy network from converging to trivial behaviors, such as consistently selecting only a subset of actions, we introduce balance loss L_b :

$$L_b = \sum_{k \in A} \mathbb{E} \left[\frac{1}{T} \sum_{t=1}^T \mathbb{I}(k_t = k) - \frac{1}{\|A\|} \right], \quad (10)$$

where $k_t \in \{1, 3, 5, 7\}$ is the action selected at time step t , T denotes the total number of time steps, and $\mathbb{I}(\cdot)$ is the indicator function.

To promote computational efficiency while preserving accuracy, we also include a Giga Floating-point Operations (GFLOPs) loss L_g , which penalizes the average computational cost:

$$L_g = \frac{1}{T} \sum_{t=1}^T \text{GFLOPs}(f_s(x_i^{\text{mixup}})), \quad (11)$$

where GFLOPs are computed based on the inference cost of the feature extraction network f_s . Thus, L_g reflects the average computational complexity over the input video V .

2) *Stage 2*: We adopt the loss functions used in YOLOv8 [21]. Specifically, the Binary Cross-Entropy (BCE) loss is applied to the classification branch, while the Distribution Focal Loss (DFL) [53] and Complete Intersection over Union (CIoU) loss [54] are employed for the regression branch.

The BCE loss function is defined as:

$$\text{Loss}_{\text{BCE}} = -w [y_n \log x_n + (1 - y_n) \log(1 - x_n)], \quad (12)$$

where w is a weighting factor, y_n denotes the ground truth label, and x_n represents the predicted value of the model.

The Distribution Focal Loss (DFL) is defined as follows:

$$\text{Loss}_{\text{DF}} = - \left[(y_{n+1} - y) \log \frac{y_{n+1} - y_n}{y_{n+1} - y} + (y - y_n) \log \frac{y - y_n}{y_{n+1} - y_n} \right]. \quad (13)$$

where y is the target continuous value, and y_n, y_{n+1} are its adjacent discrete bins.

In addition, the Complete Intersection over Union (CIoU) loss is based on the Distance-IoU (DIoU) loss [55] by introducing an additional penalty term that considers the aspect ratio consistency between the predicted bounding box and the ground truth. The CIoU loss is shown as follows:

$$\text{Loss}_{\text{CIoU}} = 1 - \text{IoU} + \frac{d^2}{c^2} + \frac{v^2}{(1 - \text{IoU}) + v}, \quad (14)$$

where d is the Euclidean distance between the centers of the predicted and ground-truth boxes, and c is the diagonal length of the smallest enclosing box covering both boxes. The term

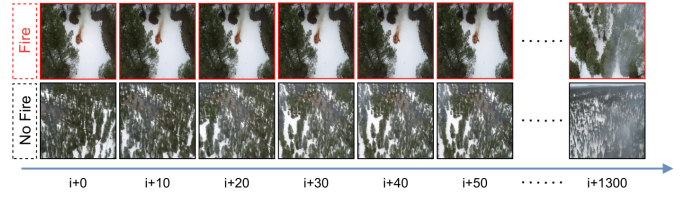


Fig. 3. A representative example illustrating the two types of labels used in the FLAME dataset [56]. The arrow indicates the temporal order of frames within a video sequence.

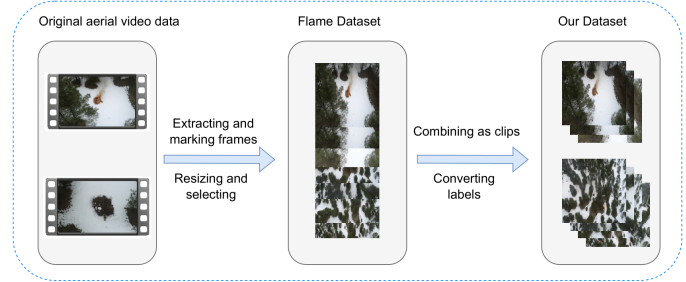


Fig. 4. The pipeline illustrating the construction process of FLAME wildfire video clips for classification tasks.

v measures the consistency of the aspect ratio and is defined as:

$$v = \frac{4}{\pi^2} \left(\arctan \frac{w_{gt}}{h_{gt}} - \arctan \frac{w_p}{h_p} \right)^2, \quad (15)$$

where w and h represent the width and height of the bounding boxes.

IV. EXPERIMENTS

A. Dataset

1) *FLAME Dataset*: The FLAME dataset [56] is a publicly available collection of wildfire images and videos captured by UAVs. For the video classification task, we utilize the seventh and eighth subsets of this dataset, comprising 39,375 images for training and validation, and 8,617 images for testing, each with a resolution of 254×254 pixels. A representative sample from this video dataset is shown in Fig. 3.

Each video sample is defined as a sequence of 64 consecutive frames extracted from the same video. If any frame within the sequence contains wildfire, the entire sample is labeled as positive. This procedure yields a curated dataset of 615 training clips and 134 testing clips, of which 483 clips contain wildfire and 266 are wildfire-free, resulting in an approximate 2:1 ratio. Example results illustrating the dataset construction process are shown in Fig. 4.

2) *HMDB51 Dataset*: The HMDB51 dataset [57] is a widely used open-domain video recognition benchmark consisting of 6,766 video clips collected from diverse real-world sources. It includes 51 distinct action categories, each containing a minimum of 101 clips. In this study, we use HMDB51 (split 1) as an auxiliary dataset to evaluate the effectiveness of our method in efficient video recognition.

3) *Fire & Smoke Dataset*: Since the FLAME and HMDB51 datasets do not include manually annotated wildfire localization, we utilize the Fire & Smoke Dataset [58] to evaluate the performance of our method in fire source localization. This dataset, published by Azimjon Akhtamov, an AI researcher at Chungbuk National University (CBNU), South Korea, contains over 17,000 images covering fire and smoke in various environments, including urban, forest, industrial, and indoor settings. It is well-suited for tasks related to early wildfire detection and Earth hazard monitoring.

B. Baseline

1) *Stage 1*: In Stage 1 of our proposed framework, we compare the performance of our frame selection method against three baselines: random frame selection, uniform frame selection, and the state-of-the-art (SOTA) method SMART [31]. In random selection, frames are sampled randomly across the entire video, while uniform selection samples frames at evenly spaced frames. For SMART, once the frames are selected, the final prediction is obtained by average pooling the outputs of one of the expensive backbones applied to each selected frame.

2) *Stage 2*: In Stage 2 of our method, we use the original YOLOv8 [21] as the baseline model and compare its performance with our improved variants: YOLOv8+ECA, YOLOv8+SA, and YOLOv8+ResCBAM.

C. Implementation Details

1) *Stage 1*: We set the number of station points to 2 and the clip mixup hyperparameter α to 0.3. To improve computational efficiency, we adopt MobileNetV2 [59] as the backbone for the feature extractor f_s , which is also used to process the station points. The Gated Recurrent Unit (GRU) [60] has a hidden dimension of 512 and consists of a single layer.

The training pipeline consists of three stages. We first fine-tune MobileNetV2, pretrained on ImageNet [61], using frame-level labels for 100 epochs. The initial learning rate is set to 0.01 and decays by a factor of 10 at epochs 50, 70, and 90. Then MobileNetV2 is frozen, and the GRU is trained using clip-level labels for 20 epochs with an initial learning rate of $1.45e-5$. Finally, both MobileNetV2 and the GRU are frozen, and the policy network is trained independently with an initial learning rate of 0.01.

To guide frame selection, we compute preference scores using a_i^{gm} . To evaluate the effectiveness of the selected frames, we train ResNet18-TSM [62], [63] for 10 epochs with an initial learning rate of 0.001 and a weight decay of $3e-6$.

2) *Stage 2*: For Stage 2 of our method, all models were trained using Python on the PyTorch framework. Experiments were conducted on an NVIDIA GeForce RTX 4090 GPU, with the batch size set to 16 to accommodate memory constraints.

For training hyperparameters, we follow the configuration used by Ju *et al.* [51], [52], employing Stochastic Gradient Descent (SGD) [64] as the optimizer. The weight decay is set to $5e-4$, with a momentum of 0.937. The initial learning rate is set to $1e-2$, and training is performed for 100 epochs.

D. Evaluation Metrics

1) *Stage 1*: For Stage 1 of our method, classification accuracy is consistently used as the primary evaluation metric for the video classification task. Accuracy is defined as the ratio of correctly predicted samples to the total number of samples and is computed as:

$$\text{Accuracy} = \frac{TP + TN}{TP + TN + FP + FN}, \quad (16)$$

where TP , TN , FP , and FN represent true positives, true negatives, false positives, and false negatives, respectively.

In addition to accuracy, we evaluate the computational cost of each model in terms of floating-point operations (FLOPs).

2) *Stage 2*: The F-score is a widely used metric for evaluating the performance of object detection models, as it incorporates both precision and recall to provide a balanced assessment of accuracy. The F-score is computed using the following equation:

$$\text{F-Score} = \frac{(1 + \beta^2) \times \text{Precision} \times \text{Recall}}{\beta^2 \times \text{Precision} + \text{Recall}}, \quad (17)$$

When $\beta = 1$, the F-score becomes the F1-score, which assigns equal weight to precision and recall and is interpreted as their harmonic mean. The F1-score is calculated as follows:

$$\begin{aligned} \text{F1-Score} &= \frac{2 \times \text{Precision} \times \text{Recall}}{\text{Precision} + \text{Recall}} \\ &= \frac{2TP}{2TP + FP + FN}, \end{aligned} \quad (18)$$

where TP , TN , FP , and FN denote true positives, true negatives, false positives, and false negatives, respectively.

Mean Average Precision (mAP) is a widely used evaluation metric in object detection tasks, providing a comprehensive measure of a model's performance across all classes. In this work, we adopt mAP@50 as the evaluation metric, where mAP@50 refers to the mean of the average precision for each class computed at an Intersection over Union (IoU) threshold of 0.5.

In addition, we report the inference time of each model, measured in milliseconds (ms). Inference time refers to the total duration required by the YOLO models to process a wildfire frame, from input through pre-processing, model inference, and post-processing, until the final prediction is obtained.

E. Quantitative Comparison for Stage 1

The distilled dataset is used to train the Temporal Shift Module (TSM) [63], a state-of-the-art (SOTA) classification model, to evaluate the effectiveness of our frame selection method. The corresponding results are summarized in Table I.

As shown in Table I, our method achieves superior performance by maintaining high classification accuracy using only 8 frames, outperforming even the results obtained from processing the full video. In addition, our method significantly outperforms the baseline methods (Uniform and Random) as well as the SOTA method SMART [31] when using the same number of frames. These results indicate that our method effectively selects the most representative frames, enabling more efficient and accurate classification of wildfire videos.

TABLE I
QUANTITATIVE COMPARISON (ACCURACY) OF TEMPORAL SHIFT MODULE (TSM) MODELS TRAINED WITH DIFFERENT NUMBERS OF SELECTED FRAMES, EVALUATED ON THE FLAME DATASET [56].

Method	Number of Frame		
	8	20	28
Uniform	87.3%	88.1%	84.3%
Random	85.1%	88.1%	86.6%
SMART	84.3%	88.1%	88.8%
Ours	87.3%	91.0%	91.0%

The highest accuracy in each group is highlighted in **bold**.

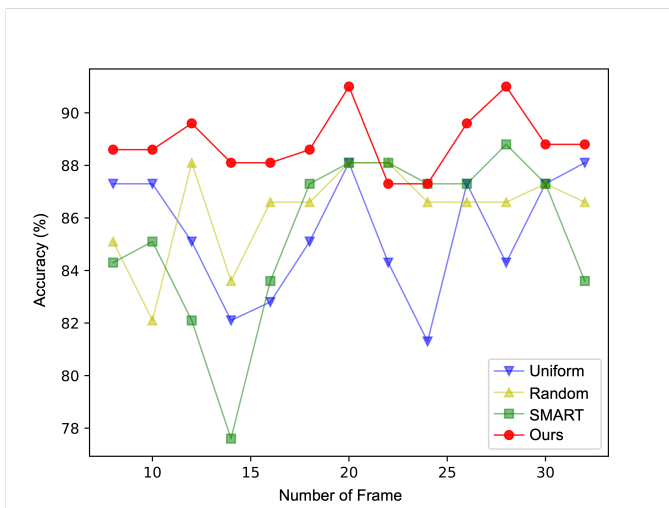


Fig. 5. Comparison of baseline methods (Uniform and Random), the SOTA method SMART [31], and our method across different numbers of selected frames, evaluated on the FLAME dataset [56].

F. Analysis of the Behavior of Frame Selection

As illustrated in Fig. 5, additional experiments are conducted across a wider range of frame counts to assess whether the observed results are affected by data randomness due to the limited dataset size. The results show that our method consistently outperforms the other three frame selection methods.

Across nearly all frame counts, our method achieves the highest classification accuracy, maintaining performance within the 88–91% range, which highlights both robustness and stability. In contrast, the performance of the other methods exhibits greater variability, particularly SMART and Random, which suffer substantial accuracy drops when the number of selected frames is small (e.g., 14 frames).

Among all methods, our method exhibits the smoothest performance curve, reflecting strong generalization capabilities with respect to varying frame numbers. By comparison, the other methods show pronounced fluctuations, with the Random method showing the highest sensitivity to the number of selected frames.

G. Ablation Study for Stage 1

To evaluate the effectiveness of the proposed method, we integrate both the feature extraction network f_s and the frame selection policy π for video classification, and compare the results with those of a baseline GRU model that relies solely on f_s . The results are summarized in Table II.

TABLE II
ABLATION STUDY OF VIDEO CLASSIFICATION PERFORMANCE (ACCURACY IN %) ON THE FLAME [56] AND HMDB51 [57] DATASETS.

Method	FLAME				HMDB51			
	Test Acc.	Train Acc.	FLOPs /Video	FLOPs /Frame	Test Acc.	Train Acc.	FLOPs /Video	FLOPs /Frame
GRU	79.10%	98.61%	26.28G	0.411G	40.72%	95.78%	30.19G	0.32G
GRU+ π	82.84%	97.40%	2.79G	0.044G	38.50%	92.34%	1.29G	0.013G

The better value in each comparison group is highlighted in **bold**.

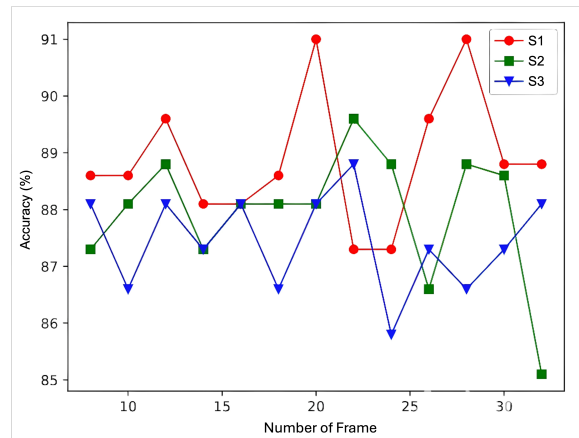


Fig. 6. Performance comparison of frame selection scoring methods S1, S2, and S3, corresponding to the scores a_i^{gm} from Eq. (5), a_i^p from Eq. (4), and a_i^{gs} from Eq. (7), respectively.

On the FLAME dataset, our method (GRU + policy) not only achieves a notable improvement in test accuracy (82.84% vs. 79.10%) but also significantly reduces computational cost. Specifically, the video-level FLOPs are reduced from 26.28G to 2.79G, and frame-level FLOPs from 0.411G to 0.044G, representing a remarkable reduction. These results highlight the effectiveness of the learned policy in identifying and focusing on informative frames, thus enhancing both accuracy and efficiency.

To further assess the generalizability of our method, we evaluate it on the HMDB51 dataset. As shown in Table II, although the test accuracy decreases slightly (from 40.72% to 38.50%), the computational cost is drastically reduced. Video-level FLOPs drop from 30.19G to 1.29G, and frame-level FLOPs from 0.32G to 0.013G, yielding a 23-fold improvement in efficiency. These results demonstrate the strong generalizability and scalability of our method across diverse video datasets.

H. Hyperparameter Experiment for Stage 1

1) *Effect of Preference Score*: In addition to using the score a_i^{gm} defined in Eq. (5) for frame selection, we further investigate two alternative scoring strategies: a_i^p from Eq.(4) and a_i^{gs} from Eq.(7). These scoring methods are referred to as S1, S2, and S3, respectively. To evaluate their effectiveness, we conduct a series of experiments varying the number of selected frames. The results are presented in Fig.6.

As shown in Fig.6, the S1-based method consistently achieves higher accuracy across most configurations compared

TABLE III
PERFORMANCE COMPARISON OF VIDEO CLASSIFICATION WITH
DIFFERENT ACTION SPACE A .

A	Test Acc.	Train Acc.	FLOPs/Video	FLOPs/Frame
{1, 3, 5}	82.84%	97.24%	3.41G	0.053G
{1, 3, 5, 7, 9}	77.60%	97.56%	3.26G	0.051G
{1, 3, 5, 7}	82.84%	97.40%	2.79G	0.044G

{1, 3, 5} corresponds to $R = \{224, 168, 112\}$.

{1, 3, 5, 7, 9} corresponds to $R = \{224, 168, 140, 112, 84\}$.

The best value in each comparison group is highlighted in **bold**.

TABLE IV
PERFORMANCE COMPARISON OF VIDEO CLASSIFICATION WITH
DIFFERENT VALUES OF THE CLIP MIXUP PARAMETER α .

α	Test Acc.	Train Acc.	FLOPs/Video	FLOPs/Frame
0.2	80.60%	97.07%	2.827G	0.0442G
0.3	82.84%	97.40%	2.792G	0.0440G
0.4	82.84%	97.07%	2.831G	0.0400G
0.5	81.36%	97.24%	2.811G	0.0439G

The best value in each comparison group is highlighted in **bold**.

to S2 and S3. Notably, S1 demonstrates more stable and superior performance, maintaining accuracy above 88% in most cases and reaching a peak of over 91%. In contrast, S2 and S3 exhibit greater variability and lower peak accuracy. These results underscore the advantage of using a_i^{gm} for frame scoring. Therefore, we adopt S1 as the scoring strategy in our proposed model to ensure optimal and reliable performance.

2) *Effect of Action Space*: We evaluate the impact of different action space configurations A on video classification performance, with the results summarized in Table III. The analysis shows that the configuration {1, 3, 5, 7} achieves the highest test accuracy while maintaining low computational cost. In contrast, expanding the action space to {1, 3, 5, 7, 9} increases FLOPs and decreases test accuracy, suggesting that a larger action space may lead the policy network to adopt a more conservative selection strategy.

3) *Effect of Clip Mixup Parameter λ* : Variations in the clip mixup parameter α affect the mixing coefficient λ , influencing model performance. As shown in Table IV, the model demonstrates relatively low sensitivity to changes in α , with optimal performance across all evaluation metrics achieved at $\alpha = 0.3$.

4) *Effect of Station Point*: We investigate the impact of different number of station points on the video classification performance, with the results summarized in Table V. The policy network exhibits substantial performance differences with and without station points. Introducing a single station point yields a 5% improvement in test accuracy while significantly reducing FLOPs. In contrast, the policy network without station points adopts a more conservative strategy. As the number of station points increases, the network tends to fuse more frames. Overall, using two station points achieves an optimal balance between computational cost and classification accuracy.

I. Quantitative Comparison for Stage 2

For the fire source detection task, we set all input image sizes to 1024 to enable a fair comparison between the baseline and the proposed methods. We evaluate two model scales:

TABLE V
PERFORMANCE COMPARISON OF VIDEO CLASSIFICATION WITH
DIFFERENT NUMBERS OF THE STATION POINTS.

	Test Acc.	Train Acc.	FLOPs/Video	FLOPs/Frame
0	75.37%	98.2%	6.61G	0.103G
1	80.60%	98.1%	2.54G	0.040G
2	82.84%	97.4%	2.79G	0.044G
3	78.36%	97.7%	3.06G	0.048G

The best value in each comparison group is highlighted in **bold**.

TABLE VI
QUANTITATIVE COMPARISON OF FIRE SOURCE DETECTION ON THE FIRE
& SMOKE DATASET USING YOLOv8 AND OUR MODELS WITH MODEL
SIZE SMALL AND INPUT IMAGE SIZE SET TO 1024.

Model	Params	FLOPs	F1	mAP@50	Inference ¹
YOLOv8	11.14M	28.6G	0.63	65.5%	1.8ms
YOLOv8+SA	11.14M	28.7G	0.64	65.2%	1.9ms
YOLOv8+ECA	11.14M	28.7G	0.64	66.0%	1.8ms
YOLOv8+ResCBAM	16.06M	38.3G	0.64	66.0%	2.1ms

¹Inference means the inference time per image measured using NVIDIA GeForce RTX 4090 GPU.

Small (S) and Medium (M), with results presented in Tables VI and VII.

In the Small model setting, both YOLOv8+SA and YOLOv8+ResCBAM outperform the original YOLOv8, which achieves 65.5% mAP@50. Specifically, both YOLOv8+ECA and YOLOv8+ResCBAM obtain mAP@50 values of 66.0%. Moreover, the inference times remain efficient: YOLOv8+ECA matches the baseline with an inference time of 1.8ms, while YOLOv8+ResCBAM suffers only a slight increase to 2.1ms. Considering model complexity, including the number of parameters and FLOPs, we select YOLOv8+ECA-S as the preferred model for fire source detection on resource-limited platforms.

On platforms with greater computational resources, the Medium model version is preferred, as it achieves higher mAP@50 values compared to the Small version. As shown in Tables VI and VII, the mAP@50 of the baseline YOLOv8 increases from 65.5% (Small) to 65.8% (Medium), accompanied by a rise in inference time from 1.8ms to 6.1ms. All of our model variants demonstrate improved performance. Notably, YOLOv8+ECA achieves 66.2% mAP@50 with only slight increases in parameters, FLOPs, and inference time. YOLOv8+ResCBAM achieves the highest accuracy of 66.6% mAP@50, though with increased complexity, its parameter count rises from 25.86M to 33.83M, FLOPs from 79.1G to 98.2G, and inference time from 6.1ms to 6.9ms. Therefore, if model accuracy is the primary consideration, YOLOv8+ResCBAM-M is the most suitable choice for fire source detection in high computing resources environments.

J. Analysis of the P-R Curve of Fire Source Detection

The Precision-Recall (P-R) Curve plots Recall on the x-axis and Precision on the y-axis, with each point corresponding to a different confidence threshold, forming a continuous curve. We generate P-R Curves for the Medium versions of various models and report fire source detection performance (mAP@50) for two classes: fire and smoke, as well as

TABLE VII
QUANTITATIVE COMPARISON OF FIRE SOURCE DETECTION ON THE FIRE & SMOKE DATASET USING YOLOv8 AND OUR MODELS WITH MODEL SIZE MEDIUM AND INPUT IMAGE SIZE SET TO 1024.

Model	Params	FLOPs	F1	mAP@50	Inference ¹
YOLOv8	25.86M	79.1G	0.64	65.8%	6.1ms
YOLOv8+SA	25.86M	79.1G	0.64	65.9%	6.3ms
YOLOv8+ECA	25.86M	79.1G	0.64	66.2%	6.1ms
YOLOv8+ResCBAM	33.83M	98.2G	0.65	66.6%	6.9ms

¹Inference means the inference time per image measured using NVIDIA GeForce RTX 4090 GPU.

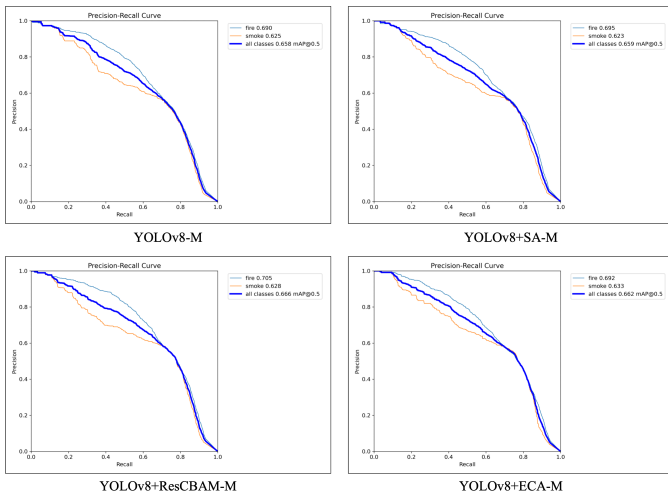


Fig. 7. Detailed Precision–Recall curves for four different models across each class in the Fire & Smoke Dataset [58].

the overall performance across all classes, as illustrated in Fig. 7. Among the models, YOLOv8+ResCBAM-M achieves the highest performance in detecting the “fire” class, with a mAP@50 of 70.5%, while YOLOv8+ECA-M performs best in detecting the “smoke” class, reaching a mAP@50 of 63.3%. In addition, all P-R Curves exhibit a steep drop, indicating a significant decline in Precision at high Recall levels. Compared to fire detection, the performance on smoke detection remains relatively lower, which still has potential to be improved.

V. DISCUSSION

In Stage 1 of our method, we further investigate the incorporation of attention-based architectures as feature extractors within the TSM framework by replacing conventional CNNs with CrossFormer [65]. Two configurations are set as: one with the CrossFormer backbone frozen and another with its parameters fully trainable. As shown in Table VIII, the trainable CrossFormer consistently outperforms the frozen version, highlighting the benefits of end-to-end optimization across all frame settings.

Nevertheless, the performance gains from this architectural enhancement remain relatively modest. Notably, increasing the number of selected frames from 20 to 28 does not yield significant improvements and, in some cases, results in a slight decrease in accuracy. This trend suggests that the representational capacity of CrossFormer may be underutilized due to the limited size of the FLAME dataset.

TABLE VIII
QUANTITATIVE COMPARISON (ACCURACY IN %) OF CROSSFORMER-TSM MODELS TRAINED WITH DIFFERENT NUMBERS OF SELECTED FRAMES.

Method	Number of Frame		
	8	20	28
Frozen CrossFormer	84.4%	85.3%	85.3%
Trained CrossFormer	86.8%	88.2%	87.4%

To further enhance model performance, especially when leveraging complex attention-based architectures, we posit that training on a larger-scale dataset is essential. Such a dataset would provide the diversity and volume necessary to mitigate underfitting and to fully exploit the expressive power of models like CrossFormer within the TSM framework.

VI. CONCLUSION AND FUTURE WORK

In this work, we propose a lightweight and efficient two-stage framework for wildfire monitoring and detection. In Stage 1, we introduce a novel method to enhance the efficiency of aerial video understanding in wildfire monitoring. In Stage 2, we employ improved YOLOv8 models for accurate fire source localization. Experiments demonstrate that our method outperforms several baseline method in Stage 1, providing a high-quality distilled dataset that enables the Temporal Shift Module (TSM) to achieve high accuracy with significantly reduced computational cost. Notably, the compression mechanism in Stage 1 is model-independent and compatible with various backbone architectures, making it broadly applicable to video-based disaster response scenarios. In Stage 2, our improved YOLOv8 models can improve mAP@50 performance while maintaining similar levels of model parameters, FLOPs, and inference time.

However, Stage 1 of our proposed framework is currently not yet suitable for real-time deployment due to its reliance on future frames for stable inference, which causes delays. In addition, the clip mixup strategy, compressing only two frames per clip, may result in feature loss. To overcome these limitations, our future work will focus on developing stable inference that do not depend on future frames, and on designing more advanced frame compression techniques capable of integrating multiple frames while preserving computational efficiency. We also plan to evaluate our framework on additional aerial video datasets to further validate its generalizability and practical applicability.

ACKNOWLEDGMENT

This research was supported by Public Computing Cloud, Renmin University of China. This work was supported by JSPS KAKENHI (Grants-in-Aid for Scientific Research, 21H05001).

REFERENCES

- [1] A. Bouguettaya, H. Zarzour, A. M. Taberkit, and A. Kechida, “A review on early wildfire detection from unmanned aerial vehicles using deep learning-based computer vision algorithms,” *Signal Processing*, vol. 190, p. 108309, 2022.
- [2] R. Nagasawa, E. Mas, L. Moya, and S. Koshimura, “Multi-uav path planning methodology for postdisaster building damage surveying,” 2020.

- [3] O. Ozkan, "Optimization of the distance-constrained multi-based multi-uav routing problem with simulated annealing and local search-based matheuristic to detect forest fires: The case of turkey," *Applied Soft Computing*, vol. 113, p. 108015, 2021.
- [4] R. Nagasawa, E. Mas, L. Moya, and S. Koshimura, "Model-based analysis of multi-uav path planning for surveying postdisaster building damage," *Scientific reports*, vol. 11, no. 1, pp. 1–14, 2021.
- [5] D. Rashkovetsky, F. Mauracher, M. Langer, and M. Schmitt, "Wild-fire detection from multisensor satellite imagery using deep semantic segmentation," *IEEE Journal of Selected Topics in Applied Earth Observations and Remote Sensing*, vol. 14, pp. 7001–7016, 2021.
- [6] S. Goyal, M. Shagill, A. Kaur, H. Vohra, and A. Singh, "A yolo based technique for early forest fire detection," *Int. J. Innov. Technol. Explor. Eng. (IJITEE) Vol.*, no. 9, pp. 1357–1362, 2020.
- [7] D. Alexandrov, E. Pertseva, I. Berman, I. Pantiukhin, and A. Kapitonov, "Analysis of machine learning methods for wildfire security monitoring with an unmanned aerial vehicles," in *2019 24th conference of open innovations association (FRUCT)*, pp. 3–9, IEEE, 2019.
- [8] F. A. Hossain, Y. M. Zhang, and M. A. Tonima, "Forest fire flame and smoke detection from uav-captured images using fire-specific color features and multi-color space local binary pattern," *Journal of Unmanned Vehicle Systems*, vol. 8, no. 4, pp. 285–309, 2020.
- [9] J. Zhan, Y. Hu, W. Cai, G. Zhou, and L. Li, "Pdam-stpnnet: a small target detection approach for wildland fire smoke through remote sensing images," *Symmetry*, vol. 13, no. 12, p. 2260, 2021.
- [10] L. Zhao, J. Hu, J. Bi, Y. Bai, E. Mas, and S. Koshimura, "Streamlining forest wildfire surveillance: Ai-enhanced uavs utilizing the flame aerial video dataset for lightweight and efficient monitoring," in *2024 IEEE/RSJ International Conference on Intelligent Robots and Systems (IROS)*, pp. 8063–8068, IEEE, 2024.
- [11] S. Koshimura and E. Mas, "Digital twin computing for enhancing resilience of disaster response system," in *EGU General Assembly Conference Abstracts*, pp. EGU–11756, 2023.
- [12] A. Piergiovanni, A. Angelova, and M. S. Ryoou, "Tiny video networks," *Applied AI Letters*, vol. 3, no. 1, p. e38, 2022.
- [13] D. Tran, H. Wang, L. Torresani, and M. Feiszli, "Video classification with channel-separated convolutional networks," in *Proceedings of the IEEE/CVF International Conference on Computer Vision*, pp. 5552–5561, 2019.
- [14] S. Liu, J. Cheng, L. Liang, H. Bai, and W. Dang, "Light-weight semantic segmentation network for uav remote sensing images," *IEEE Journal of Selected Topics in Applied Earth Observations and Remote Sensing*, vol. 14, pp. 8287–8296, 2021.
- [15] C. Guo, B. Zhao, and Y. Bai, "Deepcore: A comprehensive library for coresets selection in deep learning," *DEXA*, 2022.
- [16] Y. Meng, C.-C. Lin, R. Panda, P. Sattigeri, L. Karlinsky, A. Oliva, K. Saenko, and R. Feris, "Ar-net: Adaptive frame resolution for efficient action recognition," in *European Conference on Computer Vision*, pp. 86–104, Springer, 2020.
- [17] Y. Bai, X. Wu, L. Xu, J. Pei, E. Mas, and S. Koshimura, "Towards efficient disaster response via cost-effective unbiased class rate estimation through neyman allocation stratified sampling active learning," *arXiv preprint arXiv:2405.17734*, 2024.
- [18] G. Lin, Y. Zhang, G. Xu, and Q. Zhang, "Smoke detection on video sequences using 3d convolutional neural networks," *Fire Technology*, vol. 55, pp. 1827–1847, 2019.
- [19] S. Koshimura and S. Hayashi, "Tsunami flow measurement using the video recorded during the 2011 tohoku tsunami attack," in *2012 IEEE International Geoscience and Remote Sensing Symposium*, pp. 6693–6696, IEEE, 2012.
- [20] S. Koshimura and T. Fukuoka, "Remote sensing approach for mapping and monitoring tsunami debris," in *IGARSS 2019-2019 IEEE International Geoscience and Remote Sensing Symposium*, pp. 4829–4832, IEEE, 2019.
- [21] G. Jocher, A. Chaurasia, and J. Qiu, "Yolo by ultralytics," *Code repository*, 2023.
- [22] J. Lin, H. Duan, K. Chen, D. Lin, and L. Wang, "Ocsampler: Compressing videos to one clip with single-step sampling," in *Proceedings of the IEEE/CVF Conference on Computer Vision and Pattern Recognition*, pp. 13894–13903, 2022.
- [23] Z. Wu, C. Xiong, C.-Y. Ma, R. Socher, and L. S. Davis, "Adaframe: Adaptive frame selection for fast video recognition," in *Proceedings of the IEEE/CVF Conference on Computer Vision and Pattern Recognition*, pp. 1278–1287, 2019.
- [24] X. Sun, R. Panda, C.-F. R. Chen, A. Oliva, R. Feris, and K. Saenko, "Dynamic network quantization for efficient video inference," in *Proceedings of the IEEE/CVF International Conference on Computer Vision*, pp. 7375–7385, 2021.
- [25] B. Korbar, D. Tran, and L. Torresani, "Scsampler: Sampling salient clips from video for efficient action recognition," in *Proceedings of the IEEE/CVF International Conference on Computer Vision*, pp. 6232–6242, 2019.
- [26] Y. Meng, R. Panda, C.-C. Lin, P. Sattigeri, L. Karlinsky, K. Saenko, A. Oliva, and R. Feris, "Adafuse: Adaptive temporal fusion network for efficient action recognition," *arXiv preprint arXiv:2102.05775*, 2021.
- [27] F. Caba Heilbron, V. Escorcia, B. Ghanem, and J. Carlos Niebles, "Activitynet: A large-scale video benchmark for human activity understanding," in *Proceedings of the IEEE conference on computer vision and pattern recognition*, pp. 961–970, 2015.
- [28] Y.-G. Jiang, Z. Wu, J. Wang, X. Xue, and S.-F. Chang, "Exploiting feature and class relationships in video categorization with regularized deep neural networks," *IEEE transactions on pattern analysis and machine intelligence*, vol. 40, no. 2, pp. 352–364, 2017.
- [29] W. Kay, J. Carreira, K. Simonyan, B. Zhang, C. Hillier, S. Vijayanarasimhan, F. Viola, T. Green, T. Back, P. Natsev, et al., "The kinetics human action video dataset," *arXiv preprint arXiv:1705.06950*, 2017.
- [30] S. Yeung, O. Russakovsky, G. Mori, and L. Fei-Fei, "End-to-end learning of action detection from frame glimpses in videos," in *Proceedings of the IEEE conference on computer vision and pattern recognition*, pp. 2678–2687, 2016.
- [31] S. N. Gowda, M. Rohrbach, and L. Sevilla-Lara, "Smart frame selection for action recognition," in *Proceedings of the AAAI Conference on Artificial Intelligence*, vol. 35, pp. 1451–1459, 2021.
- [32] Y. Zhi, Z. Tong, L. Wang, and G. Wu, "Mgsampler: An explainable sampling strategy for video action recognition," in *Proceedings of the IEEE/CVF International Conference on Computer Vision*, pp. 1513–1522, 2021.
- [33] E. Casas, L. Ramos, E. Bendek, and F. Rivas-Echeverría, "Assessing the effectiveness of yolo architectures for smoke and wildfire detection," *IEEE Access*, vol. 11, pp. 96554–96583, 2023.
- [34] L. T. Ramos, E. Casas, C. Romero, F. Rivas-Echeverría, and E. Bendek, "A study of yolo architectures for wildfire and smoke detection in ground and aerial imagery," *Results in Engineering*, vol. 26, p. 104869, 2025.
- [35] J. Hu, L. Shen, and G. Sun, "Squeeze-and-excitation networks," in *Proceedings of the IEEE conference on computer vision and pattern recognition*, pp. 7132–7141, 2018.
- [36] S. Woo, J. Park, J.-Y. Lee, and I. S. Kweon, "Cbam: Convolutional block attention module," in *Proceedings of the European conference on computer vision (ECCV)*, pp. 3–19, 2018.
- [37] Q. Wang, B. Wu, P. Zhu, P. Li, W. Zuo, and Q. Hu, "Eca-net: Efficient channel attention for deep convolutional neural networks," in *Proceedings of the IEEE/CVF conference on computer vision and pattern recognition*, pp. 11534–11542, 2020.
- [38] Q.-L. Zhang and Y.-B. Yang, "Sa-net: Shuffle attention for deep convolutional neural networks," in *ICASSP 2021-2021 IEEE International Conference on Acoustics, Speech and Signal Processing (ICASSP)*, pp. 2235–2239, IEEE, 2021.
- [39] H. Zhang, M. Cisse, Y. N. Dauphin, and D. Lopez-Paz, "mixup: Beyond empirical risk minimization," *arXiv preprint arXiv:1710.09412*, 2017.
- [40] Y. Wu and K. He, "Group normalization," in *Proceedings of the European conference on computer vision (ECCV)*, pp. 3–19, 2018.
- [41] Z. Wu, C. Xiong, Y.-G. Jiang, and L. S. Davis, "Liteeval: A coarse-to-fine framework for resource efficient video recognition," *Advances in Neural Information Processing Systems*, vol. 32, 2019.
- [42] E. Jang, S. Gu, and B. Poole, "Categorical reparameterization with gumbel-softmax," *arXiv preprint arXiv:1611.01144*, 2016.
- [43] C.-Y. Wang, H.-Y. M. Liao, Y.-H. Wu, P.-Y. Chen, J.-W. Hsieh, and I.-H. Yeh, "Cspnet: A new backbone that can enhance learning capability of cnn," in *Proceedings of the IEEE/CVF conference on computer vision and pattern recognition workshops*, pp. 390–391, 2020.
- [44] G. Jocher, K. Nishimura, T. Mineeva, and R. Vilariño, "yolov5," *Code repository*, p. 9, 2020.
- [45] C.-Y. Wang, H.-Y. M. Liao, and I.-H. Yeh, "Designing network design strategies through gradient path analysis," *arXiv preprint arXiv:2211.04800*, 2022.
- [46] C.-Y. Wang, A. Bochkovskiy, and H.-Y. M. Liao, "Yolov7: Trainable bag-of-freebies sets new state-of-the-art for real-time object detectors," in *Proceedings of the IEEE/CVF conference on computer vision and pattern recognition*, pp. 7464–7475, 2023.
- [47] T.-Y. Lin, P. Dollár, R. Girshick, K. He, B. Hariharan, and S. Belongie, "Feature pyramid networks for object detection," in *Proceedings of the IEEE conference on computer vision and pattern recognition*, pp. 2117–2125, 2017.

- [48] S. Liu, L. Qi, H. Qin, J. Shi, and J. Jia, "Path aggregation network for instance segmentation," in *Proceedings of the IEEE conference on computer vision and pattern recognition*, pp. 8759–8768, 2018.
- [49] S. Ren, K. He, R. Girshick, and J. Sun, "Faster r-cnn: Towards real-time object detection with region proposal networks," *Advances in neural information processing systems*, vol. 28, 2015.
- [50] K. Duan, S. Bai, L. Xie, H. Qi, Q. Huang, and Q. Tian, "Centernet: Keypoint triplets for object detection," in *Proceedings of the IEEE/CVF international conference on computer vision*, pp. 6569–6578, 2019.
- [51] R.-Y. Ju, C.-T. Chien, and J.-S. Chiang, "Yolov8-rescbam: Yolov8 based on an effective attention module for pediatric wrist fracture detection," *arXiv preprint arXiv:2409.18826*, 2024.
- [52] C.-T. Chien, R.-Y. Ju, K.-Y. Chou, E. Xieerke, and J.-S. Chiang, "Yolov8-am: Yolov8 based on effective attention mechanisms for pediatric wrist fracture detection," *IEEE Access*, vol. 13, pp. 52461–52477, 2025.
- [53] X. Li, W. Wang, L. Wu, S. Chen, X. Hu, J. Li, J. Tang, and J. Yang, "Generalized focal loss: Learning qualified and distributed bounding boxes for dense object detection," *Advances in Neural Information Processing Systems*, vol. 33, pp. 21002–21012, 2020.
- [54] Z. Zheng, P. Wang, D. Ren, W. Liu, R. Ye, Q. Hu, and W. Zuo, "Enhancing geometric factors in model learning and inference for object detection and instance segmentation," *IEEE transactions on cybernetics*, vol. 52, no. 8, pp. 8574–8586, 2021.
- [55] Z. Zheng, P. Wang, W. Liu, J. Li, R. Ye, and D. Ren, "Distance-iou loss: Faster and better learning for bounding box regression," in *Proceedings of the AAAI conference on artificial intelligence*, vol. 34, pp. 12993–13000, 2020.
- [56] A. Shamsoshoara, F. Afghah, A. Razi, L. Zheng, P. Z. Fulé, and E. Blasch, "Aerial imagery pile burn detection using deep learning: The flame dataset," *Computer Networks*, vol. 193, p. 108001, 2021.
- [57] H. Kuehne, H. Jhuang, E. Garrote, T. Poggio, and T. Serre, "Hmdb: a large video database for human motion recognition," in *2011 International conference on computer vision*, pp. 2556–2563, IEEE, 2011.
- [58] A. Akhtamov, "Fire & smoke dataset." <https://www.kaggle.com/datasets/azimjaan21/fire-and-smoke-dataset-object-detection-yolo>, 2023.
- [59] M. Sandler, A. Howard, M. Zhu, A. Zhmoginov, and L.-C. Chen, "Mobilenetv2: Inverted residuals and linear bottlenecks," in *Proceedings of the IEEE conference on computer vision and pattern recognition*, pp. 4510–4520, 2018.
- [60] K. Cho, B. Van Merriënboer, C. Gulcehre, D. Bahdanau, F. Bougares, H. Schwenk, and Y. Bengio, "Learning phrase representations using rnn encoder-decoder for statistical machine translation," *arXiv preprint arXiv:1406.1078*, 2014.
- [61] J. Deng, W. Dong, R. Socher, L.-J. Li, K. Li, and L. Fei-Fei, "Imagenet: A large-scale hierarchical image database," in *2009 IEEE conference on computer vision and pattern recognition*, pp. 248–255, Ieee, 2009.
- [62] K. He, X. Zhang, S. Ren, and J. Sun, "Deep residual learning for image recognition," in *Proceedings of the IEEE conference on computer vision and pattern recognition*, pp. 770–778, 2016.
- [63] J. Lin, C. Gan, and S. Han, "Tsm: Temporal shift module for efficient video understanding," in *Proceedings of the IEEE/CVF International Conference on Computer Vision*, pp. 7083–7093, 2019.
- [64] S. Ruder, "An overview of gradient descent optimization algorithms," *arXiv preprint arXiv:1609.04747*, 2016.
- [65] Y. Zhang and J. Yan, "Crossformer: Transformer utilizing cross-dimension dependency for multivariate time series forecasting," in *The eleventh international conference on learning representations*, 2023.